aerospace

MDPI

Article

Radiation Hard 2.5 Gb/s InGaAs/AlGaAsSb Avalanche Photodiode for Harsh Space Environments

Ding Chen [1], Jonty Veitch [1], Jonathan Petticrew [1], Anne Samaras [2], Oliver Saint-Pe [2], Jo Shien Ng [1] and Chee Hing Tan [1,*]

[1] School of Electrical and Electronic Engineering, University of Sheffield, Sheffield S1 3JD, UK
[2] Airbus Defence and Space, 31 Rue des Cosmonautes, 31402 Toulouse, France
* Correspondence: c.h.tan@sheffield.ac.uk

Abstract

To realise high-speed free-space optical communication links in harsh space environments, it is crucial to consider the link's operating wavelength, the performance of the optical receiver, and the radiation hardness of the avalanche photodiode (APD)—optical detectors in the optical receivers. In this work, we experimentally evaluated the radiation hardness of 2.5 Gb/s receivers based on InGaAs/AlGaAsSb APDs integrated with Ommic CGY2102UH/C2 transimpedance amplifiers. Proton energy (62 MeV) and fluence (up to 3.8×10^{10} p/cm^2) representative of space environments were used to irradiate multiple receivers, ensuring rigour. After irradiation, the receivers maintained their avalanche gain and photocurrent, while exhibiting bandwidths exceeding 1.5 GHz. Despite a slight increase in APD's dark current at high reverse bias, there was no degradation of the receiver's bit error rate. At 2.5 Gb/s data rate and 1550 nm wavelength, the irradiated receivers achieved a bit error rate of 10^{-9} with an average optical power of −38.2 dBm, outperforming selected commercial receivers by ~3 dB. Since the displacement damage dose induced by the proton radiation levels used in this work are representative of those in Low Earth, Geostationary and Global Positioning System orbits, we demonstrated that InGaAs/AlGaAsSb APDs have sufficient radiation hardness to be employed as optical detectors of high-speed optical links in harsh space environments.

Keywords: AlGaAsSb; avalanche photodiodes (APDs); bit error rate (BER); free space optical communication (FSOC); optical receivers; proton irradiation; radiation hardness

Check for updates

Academic Editors: Cyril Bourgenot, Christopher Graham and Supachai Awiphan

Received: 17 April 2026
Revised: 16 May 2026
Accepted: 18 May 2026
Published: 21 May 2026

Copyright: © 2026 by the authors. Licensee MDPI, Basel, Switzerland. This article is an open access article distributed under the terms and conditions of the Creative Commons Attribution (CC BY) license.

1. Introduction

Free space optical communication (FSOC) has become a key technology for next-generation space- and ground-based communication systems because it offers increased data rates, narrower signal divergence, high security, license-free operation and immunity to electromagnetic interference compared to the traditional radio frequency (RF) communication links [1]. High-capacity, high data rate data transmission between terrestrial and spaceborne platforms therefore tend to include FSOC links. Examples include the European Data Relay System (EDRS) using FSOC to relay high-volume Earth-observation data [2] and a ground-to-satellite link for 5G Networks being planned by the European Space Agency (ESA) [3]. Another example is the TELEO mission which demonstrated FSOC at up to 9 Gb/s data rate linking between Geostationary Orbit (GEO) and Earth [4,5]. Some of the key determining factors of a FSOC link's performance are (i) operating wavelength and (ii) performance of its optical receiver, which can be characterized by its signal to

noise ratio (SNR). Although these factors are important in all optical communication links, they are particularly so in FSOC, due to long propagation and atmospheric attenuation. Additionally, FSOC receivers incorporating high gain, low-noise, uncooled avalanche photodiode (APD) can simplify the optical system and contribute to reductions in payload size and weight for space-based instruments. The optical receiver must also maintain reliable performance under demanding space and atmospheric conditions.

A commonly used operating wavelength in FSOC links is 1550 nm. Under nominal solar conditions, background radiance at 1550 nm is 6 $W/m^2/\mu m/sr$, significantly lower than those at shorter wavelengths (e.g., 42.6 $W/m^2/\mu m/sr$ at 850 nm) [6], suppressing background noise in the optical receiver. Furthermore, the wavelength of 1550 nm is eye-safe (allowing higher transceiver power) and a wide range of optical components (e.g., laser and optics) are available commercially.

Typical FSOC receivers for 1550 nm optical signals use an indium gallium arsenide (InGaAs)-based avalanche photodiode (APD) integrated with a low noise transimpedance amplifier (TIA). In the APD, its multiplication region is subjected to a high electric field, such that charged carriers generated by absorption of the optical signals grow into an avalanche of charged carriers. The signal experiences an internal gain characterized by the APD's multiplication factor, M. The multiplication process produces additional noise, characterized by excess noise factor, F, which increases with M. The exact $F(M)$ characteristics depend on the avalanche materials and the avalanche region widths.

Commercial InGaAs-based APDs mostly use indium phosphide (InP) multiplication regions [7], though some use indium aluminum arsenide (InAlAs) multiplication regions to reduce F [8]. Relative to silicon (Si), both InP and InAlAs exhibit high F at high M, limiting the receiver's SNR as shown in [9]. An emerging avalanche material is $Al_{0.85}Ga_{0.15}As_{0.56}Sb_{0.44}$ (referred to as AlGaAsSb hereafter) exhibiting Si-like low excess noise [10]. High performance AlGaAsSb APDs [11] and room temperature AlGaAsSb Geiger mode APD [12] for 1550 nm wavelength detection have been reported. Recently a low noise 2.5 Gb/s optical receiver consisting of InGaAs/AlGaAsSb APD and a low noise TIA was demonstrated [9]. The minimum required optical power, P_{opt}, to achieve a bit error rate (BER) of 10^{-9} was ~3 dB better (lower) than commercial InGaAs/InP receivers, suggesting the potential of using InGaAs/AlGaAsSb APDs for long range FSOC. To fully assess their potential for space-based FSOC applications, it is important to evaluate the radiation hardness of InGaAs/AlGaAsSb APDs, which is absent from existing literature.

Radiation hardness is a critical criterion for space applications due to the exposure to energetic particles in space compared with atmospheric environments. The radiation environment depends strongly on the orbits and mission duration. Optical terminals are typically deployed either in low earth orbit (LEO) missions with lifetimes of 5–7 years, or in geostationary orbit missions with lifetimes up to 15 years [13]. In LEO, displacement damage is dominated by trapped protons encountered during South Atlantic Anomaly passages, with proton energies ranging from hundreds of keV to several hundred MeV [14]. Trapped proton flux is negligible in GEO, however cumulative exposure to high-energy protons can lead to significant displacement damage over long mission durations [15]. According to radiation environment models (e.g., AE9/AP9), the 10-year mission-integrated integral proton fluence at energy above ~60 MeV can reach ~10^{10}–10^{11} p/cm^2 for LEO and GEO missions, depending on orbit parameters, shielding thickness and confidence level [16].

Proton irradiation was found to introduce semiconductor lattice defects in InGaAs arising from displacement damage. For instance, a packaged InGaAs photodiode-TIA receiver irradiated with 100 MeV protons at a fluence of 1.6×10^{11} p/cm^2 exhibited increased mean dark current (from 25.5 to 94.2 nA at −20 V), which was not recovered through thermal

annealing [17]. However, other key parameters, including responsivity, TIA drive current, PIN-TIA conversion gain, bandwidth, and P_{opt} remained nearly unchanged [17]. On the other hand, using extremely harsh environments (energy of 24 GeV and fluence > 10^{14} p/cm^2) resulted in increased capacitance and reduced responsivity, degrading the receiver's sensitivity performance [18]. For InGaAs-based APDs, a proton fluence of 2×10^{12} p/cm^2 at 63 MeV was found to increase dark current by 2 to 4 orders of magnitude [19].

In this work, we address proton-radiation tolerance at receiver level for receivers based on InGaAs/AlGaAsSb APDs. We investigated the effects of proton irradiation on both optical and electrical characteristics of an InGaAs/AlGaAsSb APD-TIA receiver, using irradiation conditions relevant to space applications. We also quantified the effects of proton irradiation on the receiver's P_{opt} for a BER of 10^{-9} at a data rate of 2.5 Gb/s.

2. Experimental Detail

2.1. APD-TIA Integration

InGaAs/AlGaAsSb APD dies were procured from Phlux Technology Ltd. (Sheffield, UK). The APD has a responsivity value of 0.97 A/W, using an InGaAs absorption layer and AlGaAsSb multiplication layer, with a field control layer inserted between them to achieve the required electric field profile [20]. Ti/Au metal contacts were deposited to form ohmic contacts. Each APD had an optical sensitive area with a diameter 50 µm and was integrated with an Ommic CGY2102UH/C2 TIA [21] using bond wires into a TO-46 header, as shown in Figure 1. A total of 13 headers were used in this work. The TIA has been evaluated for space applications and is listed on the ESA's European preferred parts list (see ED02AH) [22]. It used silicon nitride passivation, which is known to reduce radiation-induced leakage current [23]. It has a bandwidth of 2.8 GHz and a moderately low noise current of 3.98 pA/Hz$^{1/2}$. For optimal TIA performance, the suggested photodiode or APD capacitance is 0.3 pF, which is close to that of the APDs used. An additional reference receiver using the same APD and TIA dies was packaged with an LC (Lucent Connector) receptacle header, which is a miniature push-full fiber optic connector widely used in data centres. The header contains an internal lens to minimize optical coupling loss. All receiver characterization and tests were performed at room temperature.

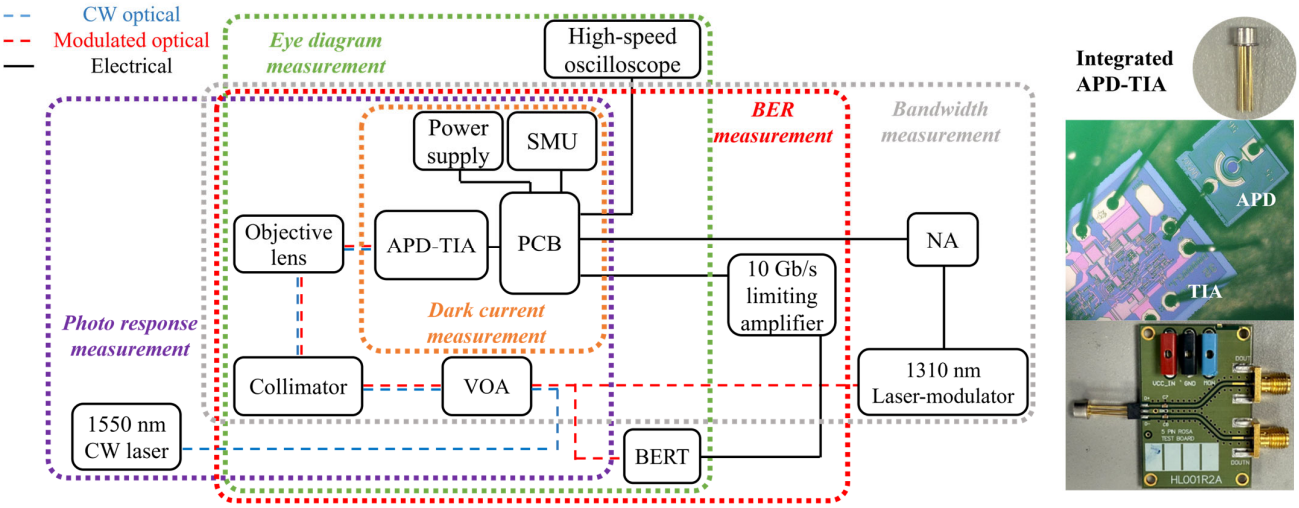

Figure 1. Integrated APD-TIA receiver and schematic diagram of measurement system used to obtain the dark current, photocurrent, bandwidth, eye diagram, and BER from the receivers. The colored dashed boxes indicate different measurements' setup.

2.2. Electrical and Optical Characterization

For each receiver, both electrical and optical characteristics were obtained in pre-irradiation (pre-rad) and post-irradiation (post-rad) measurements. The APD-TIA receiver was mounted on a printed circuit board (PCB) to facilitate measurements of dark current (I_d), photocurrent (I_{ph}), M, and BER. All measurements were conducted at room temperature using the setup shown in Figure 1, as room-temperature operation is essential for reducing the cost of integrating detectors into space-based optical terminals. The TIA was biased at 3.3 V using a DC power supply, while the APD was biased using a TTi SMU4201 source measure unit (SMU, Aim-TTi Ltd., Huntingdon, UK), which also measured the current flowing through the APD. In dark current-voltage (I-V) measurement, three sets of I-V data were taken to yield a mean I-V data for a given receiver. During the I-V measurements for the APDs, currents drawn by the TIAs were also recorded.

In photocurrent measurements, optical signals were provided by a 1550 nm wavelength fiber coupled continuous-wave laser. A collimator and an objective lens mounted on motorized translation stages helped to couple the optical signals into the receiver. The optical setup included a variable optical attenuator (VOA) for adjusting optical power on the receiver. Using a fixed optical power of −40 dBm and the reference receiver with an LC receptacle, an optical coupling loss due to the objective lens was estimated to be 0.44 dB. This loss was accounted for when measuring the APD's responsivity, R. The APD's gain, M, was deduced using $M(V) = R(\mathrm{V})/R_0$, where R_0 is the responsivity value at unity gain (0.97 A/W as provided by Phlux was used).

To characterize the receiver's bandwidth, an Agilent E8364B network analyzer (Agilent Technologies, Santa Clara, CA, USA) was used. The network analyzer's RF signal was fed to an Exail laser-modulator system (Exail, La Garde, France) to generate a 1310 nm wavelength modulated optical signal, which was subsequently focused onto the receiver. The receiver's photocurrent signal was measured by the network analyzer.

For BER measurements at 2.5 Gb/s, a BER tester (BERT, Optellent OPB02X10, Optellent Inc., Santa Rosa, CA, USA) was used to generate an optical signal with a pseudo random binary sequence, PRBS23. The receiver's response was connected to a limiting amplifier (Analog Devices MAX3945, Analog Devices Inc., Wilmington, MA, USA) before being measured by the BER tester. The corresponding optimal bias voltage for each APD was given by the reverse bias yielding the minimum BER when the optical power was fixed at −40 dBm. An example of the bias dependence of the receiver BER in this work is shown in Figure 2. The lowest BER was obtained at an optimum bias ranging from 60.2 to 60.8 V. The extinction ratio of BER tester (which directly influences BER performance) was measured to be 12 dB using a high-speed oscilloscope (Agilent 86100B, Agilent Technologies, Santa Clara, CA, USA). The oscilloscope was also used to record the eye diagram of the receivers, providing insights into the timing and noise characteristics of the receiver.

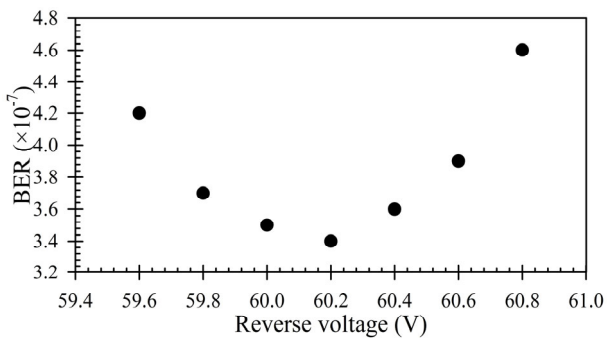

Figure 2. Measured BER of a receiver in this work at 2.5 Gb/s and a wavelength of 1550 nm, using an optical power of −40 dBm.

2.3. Radiation Test Conditions

The receivers were separated into four groups (A, B, C and D) for proton irradiation at three fluences, as shown in Table 1. Four receivers in Group D serve as reference for pre-irradiation performance. Proton irradiation was carried out at the Light Ion Facility, Université Catholique de Louvain, Belgium, using proton flux of 10^8 p/cm^2/s with the receivers unbiased, placed in three electrostatic discharge boxes and at room temperature. The proton energy of 62 MeV was selected to ensure sufficient penetration through the package with minimal interaction and a more uniform energy at the receiver. This energy also corresponds to the maximum available at the irradiation facility and minimizes the total ionizing dose effects. Since the proton beam characteristic is not expected to be altered at the header's optical window, we assumed that the APD and TIA were subjected to identical proton fluence and energy. Displacement Damage Dose (DDD), defined as the product of the non-ionizing energy loss (NIEL) and the particle fluence, is also included in Table 1 to provide a measure of the cumulative non-ionizing energy deposited in a material by energetic particles. The NIEL was calculated using codes from [24]. Post-irradiation characterization was performed after an interval of five weeks.

Table 1. Experimental proton irradiation parameters for the different APD-TIA receiver groups.

Group	Number of Receivers	Fluence (p/cm^2)	DDD (MeV/g)
A	3	3.8×10^9	3.84×10^6
B	3	1.8×10^{10}	1.82×10^7
C	3	3.8×10^{10}	3.84×10^7
D	4	(not irradiated)	(not irradiated)

The interval was necessary as a safety measure, because metals within the receivers could become radioactive following high-energy proton irradiation. Previous studies have shown room temperature annealing can partially reduce radiation-induced dark current, with the recovery magnitude depending on material and device structure. For example, some APDs showed dark current reduced by ~8% one month after irradiation, whereas others decreased by 18% after 8 days [19]. Although the interval in our work introduces some room temperature annealing, all irradiated receivers experienced the same storage interval and conditions. Hence, the relative comparison among the irradiated groups remains valid.

3. Results

3.1. Dark Current

Experimental dark currents from the 13 receivers are highly uniform, as shown in Figure 3a. After reverse bias of ~5 V, the dark current remains constant with reverse bias up to 50 V. It then rapidly increases with reverse bias at ~63–64 V, which is the apparent breakdown voltage. A separate I-V measurement without any receiver suggests that the dark current at low bias up to ~63 V (data shown in Figure 3a) may be dominated by leakage current from the PCB and/or the experimental setup. Figure 3b–d compare the pre- and post-rad dark currents for a given irradiation fluence. The breakdown voltages that can be observed from the pre- and post-rad I-V data are indistinguishable. Similarly, for bias <45 V, there is no noticeable difference between the pre-rad and post-rad I-V data. However, above 45 V, all the irradiated receivers exhibit dark currents that (i) increase gradually with APD reverse bias and (ii) are higher than pre-rad data.

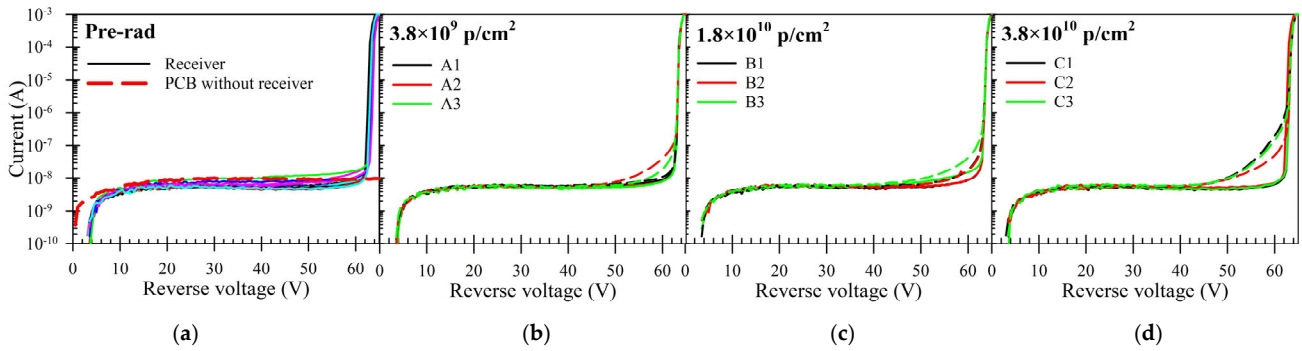

Figure 3. Pre-rad I-V characteristics of (**a**) all 13 receivers as well as comparisons before (solid lines) and after irradiation (dashed lines) using 62 MeV proton at fluence of (**b**) 3.8×10^9, (**c**) 1.8×10^{10}, and (**d**) 3.8×10^{10} p/cm^2.

To aid comparisons between the pre- and post-radiation dark currents, dark current values at 60 V (near the optimum voltage for BER; include any setup/PCB leakage) are shown in Table 2. The mean value of dark current is 8.7 nA before irradiation. Using 62 MeV protons and increasing the proton fluence from 3.8×10^9 to 3.8×10^{10} p/cm^2 increases the average dark current from 23.7 to 129 nA. On average, the dark current increased by a factor of 2.9, 2.3, and 18.8 for the three fluences (increasing order). The worst performing receiver (C3) suffered from an increase by a factor of 29.4. In contrast, the TIAs appear to be unaffected by the irradiation because the pre- and post-rad TIA currents are similar.

Table 2. Pre- and post-rad APD's dark current and avalanche gain as well as the receiver's P_{opt} (at 2.5 Gb/s and BER of 10^{-9}). * indicates the mean value from Group D (control).

Fluence (62 MeV) (p/cm^2)	Receiver	I_d at 60 V (nA)		P_{opt} at BER of 10^{-9} (dBm)		APD Gain
		Pre-Rad	Post-Rad	Pre-Rad	Post-Rad	
3.8×10^9	A1	9.0	10.9	−38.2 *	−37.8	51.9
	A2	7.9	18.9		−37.5	54.3
	A3	8.0	41.2		−37.9	50.0
1.8×10^{10}	B1	8.8	17.6		−38.1	57.2
	B2	8.9	18.1		−38.1	55.3
	B3	15.1	43.4		−39.2	57.7
3.8×10^{10}	C1	7.2	50.9		−37.6	53.2
	C2	7.1	141.0		−38.0	53.4
	C3	6.6	195.0		−38.0	52.8

3.2. Photocurrent

The I_{ph} versus reverse bias data of the 13 receivers for optical power of −40 dBm are highly uniform as shown in Figure 4a, except for the APD's punch-through voltage (the voltage at which the absorption region is fully depleted). The pre- and post-rad I_{ph} data for a given irradiation fluence are compared in Figure 4b–d. There is no significant change in the I_{ph} in all three groups. Repeating the measurements at a higher optical power of −30 dBm yielded the same observation.

M-V characteristics from pre- and post-irradiation for all fluences are compared in Figure 5. There is no significant difference in the pre- and post-rad mean gain values. Mean values of *M* at 60 V for Group A, B, and C are 48.2, 44.3, and 47.7 from the post-irradiation data, respectively. These are close to the corresponding pre-irradiation gain values of 48.7, 44.3, and 48.2, respectively.

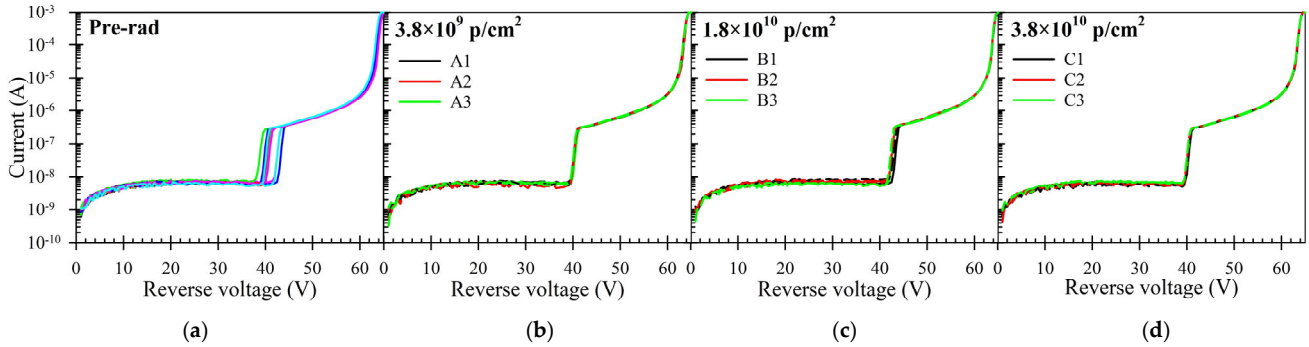

Figure 4. Pre-rad photocurrent versus reverse bias characteristics at optical power of −40 dBm of (**a**) all 13 receivers as well as comparisons before (solid lines) and after irradiation (dashed lines) using 62 MeV proton at fluence of (**b**) 3.8×10^9, (**c**) 1.8×10^{10}, and (**d**) 3.8×10^{10} p/cm^2.

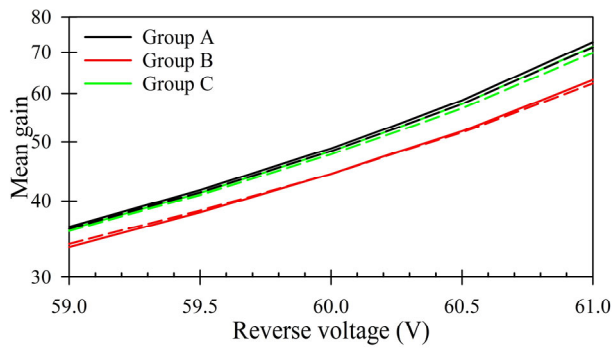

Figure 5. Mean avalanche gain extracted from pre- (solid lines) and post-rad (dashed lines) photocurrent data obtained with an optical power of −40 dBm.

Using mean I_{ph} values at −40 dBm and 46 V (after the punch through voltage), the mean responsivity values before irradiation for Group A, B, and C were 4.3, 4.1, and 4.3 A/W, respectively, compared to 4.5, 4.2, and 4.5 A/W from the post-irradiation data. Overall, both responsivity and avalanche gain of the APDs were not affected by the displacement damage caused by proton irradiation up to a fluence of 3.8×10^{10} p/cm^2. Our observations are consistent with those of [17].

3.3. Bandwidth

Prior to the irradiation campaign, frequency response measurements were performed on four receivers from Group D (not irradiated), biased at 60 V and an input optical power of −40 dBm. Since the I-V and gain data were highly similar between all receivers, we assume the bandwidths from Group D receivers are representative of a typical pre-rad bandwidth. The frequency response data from one receiver from each group, A1, B3, and C3, are compared to those from Group D in Figure 6. Although there is variation in the −3 dB bandwidths, all the values exceed 1.5 GHz, which is sufficient for 2.5 Gb/s data rate. The similarity of bandwidths from all groups suggests there was no significant change in bandwidth.

3.4. BER

Figure 7a shows the pre-rad BER as a function of optical power from Group D (control), which yield a mean P_{opt} value of -38.2 ± 0.2 dBm at BER of 10^{-9}. This is 3.5 and 3.2 dB better than commercial receivers from GoFoton [25] and Dexerials [26], respectively (as stated in their datasheets). All irradiated receivers outperform the two commercial receivers, as shown in Figure 7b–d. Compared to those of Group D, the irradiated receivers exhibit

similar or slightly worse performance (difference < 0.6 dB). The best P_{opt} value of −39.2 dBm was achieved by receiver B3. Values of P_{opt} at BER of 10^{-9} from Figure 7 are summarized in Table 2. The corresponding gain values (ranging from 50 to 57.7) to achieve the best BER are also summarized in Table 2.

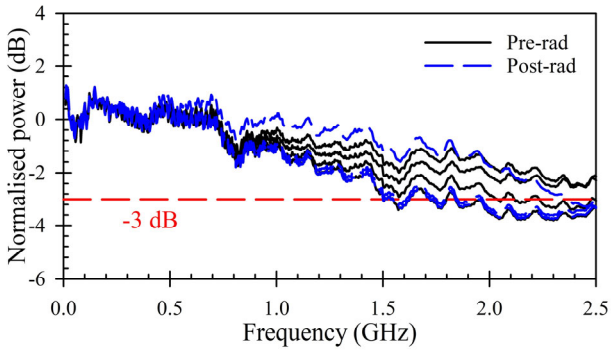

Figure 6. Normalized frequency response of four receivers without irradiation (control groups, solid lines) and one irradiated receiver in each group (dashed lines). The APD was reverse biased at 60 V and the optical signal wavelength was 1310 nm.

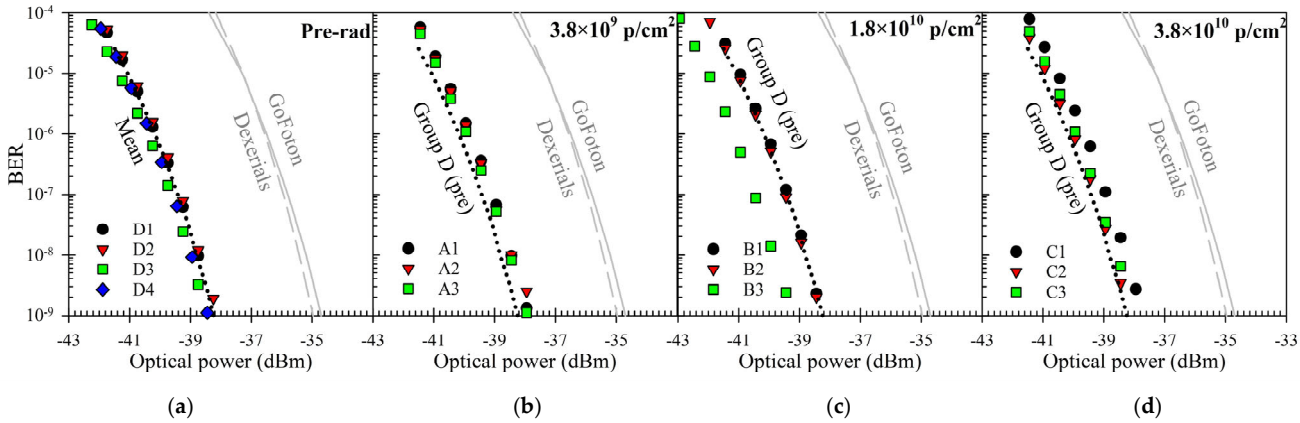

Figure 7. BER measured at 2.5 Gb/s and 1550 nm wavelength from receivers that were (**a**) not irradiated at all as well as those irradiated using 62 MeV proton at fluence of (**b**) 3.8×10^9, (**c**) 1.8×10^{10}, and (**d**) 3.8×10^{10} p/cm^2. Data from commercial receivers (GoFoton [25] and Dexerials [26]) are included for comparison.

4. Discussion

4.1. Radiation-Induced Damage Factor

Figure 8a compares average increases in dark current density for a given proton fluence at operating reverse bias for M = 10 and 50. Reported increases in InGaAs-based APDs (manufactured by PerkinElmer and Hamamatsu) from ref. [19], limited to operating condition for M = 10, are included for comparisons. At M = 10, for a given proton fluence, our receivers exhibit smaller increases in dark current than those from PerkinElmer and Hamamatsu APDs. At M = 50, our receivers behaved similarly to PerkinElmer and Hamamatsu APDs. This suggests that the InGaAs/AlGaAsSb APDs evaluated in this work can be operated at $M > 10$, offering flexibility to optimize other performance parameters.

To compare and assess the radiation hardness of receivers, the damage factor, K_{dark}, is commonly used. It is given by

$$K_{dark} = [I(\Phi) - I(0)]/\Phi A, \quad (1)$$

where Φ is the fluence, A is APD's active area, and $I(0)$ is the APD's dark current prior to irradiation. To account for differences between the receivers' operating M, normalized damage factor, K_{dark}/M can be used instead, as shown in Figure 8b. Assuming that radiation-induced degradation scales linearly with proton fluence, the results at M = 50 from Groups A and C are broadly consistent with those from PerkinElmer and Hamamatsu receivers. Group B deviates from this trend; however, the origin of this discrepancy is not fully understood. At M = 10, K_{dark}/M is lower in the receivers of this work. Without full details of these APDs (beyond the fact that APDs of this work use wide bandgap AlGaAsSb as the avalanche region), further investigations for the cause(s) of the observed differences were not possible.

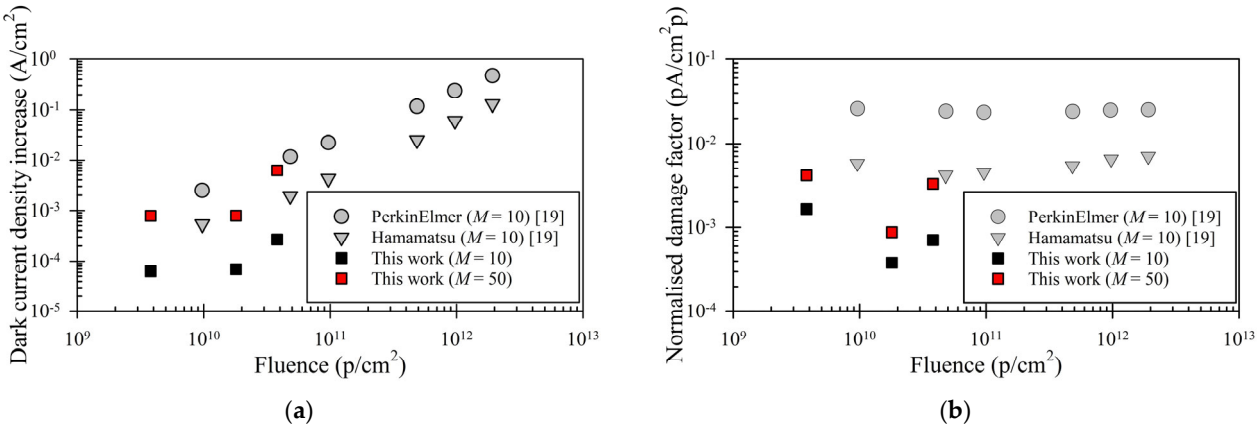

Figure 8. (**a**) Increase in dark current density and (**b**) Normalized damage factor of the receivers of this work at M = 10 and 50 (black and red symbols) and other commercial receivers at M = 10 [19] (grey symbols).

4.2. Gain and Responsivity Analysis

When a photon is absorbed outside of the photodiode depletion region, the photogenerated carriers will diffuse to the depletion region. The collection efficiency is dependent on the minority carrier diffusion length. The minority carrier diffusion length can be reduced due to displacement damage caused by sufficiently high proton irradiation, leading to reduced collection efficiency and hence reduced responsivity. However, since the InGaAs absorption layer is within the depletion region, the responsivity does not depend on minority carrier diffusion length. Therefore, the responsivity of the InGaAs/AlGaAsSb APD is not affected by the proton irradiation in this work.

The avalanche gain primarily depends on the energy gain from the electric field and energy loss through photon scattering in the AlGaAsSb multiplication layer. The dominant scattering rates in AlGaAsSb are expected to be intervalley and alloy scatterings, rather than an imperfect lattice. This could explain why the avalanche gain in AlGaAsSb is not affected by the proton irradiation in this work.

4.3. BER Analysis

For a given TIA noise, a material with lower excess noise will enable higher avalanche gain, leading to improved signal to noise performance. AlGaAsSb APDs exhibit lower excess noise than conventional InGaAs/InP and InGaAs/InAlAs APDs [9]. Consequently, the InGaAs/AlGaAsSb APD can be operated at much higher gain (50–58) compared to InP or InAlAs APDs, leading to improved BER.

Despite an increase in APD's dark current, our data show that proton irradiation has not degraded the BER performance, consistent with that reported in [17]. This suggests that the noise associated with the APD's dark current was negligible compared to other

noise sources, e.g., shot noise from the multiplied photocurrent, the TIA or the system. We note that the TIA's total input noise current is 207 nA, higher than the irradiated APD's dark current (shown in Table 2) at operating conditions.

Receiver B3 exhibited BER superior to those of all other receivers (including those in the control group), so we carried out additional eye-diagram measurements for receiver B3 and another receiver, D3 (selected from the control group). The eye-diagrams of receiver B3 and D3 measured without a limiting amplifier are shown in Figure 9. Both receivers produced comparable eye widths but B3 showed a significantly greater eye amplitude of 38.9 mV, compared to 27.9 mV in D3. Consequently, B3 achieved a higher SNR of 6.27, compared to 4.43 in D3.

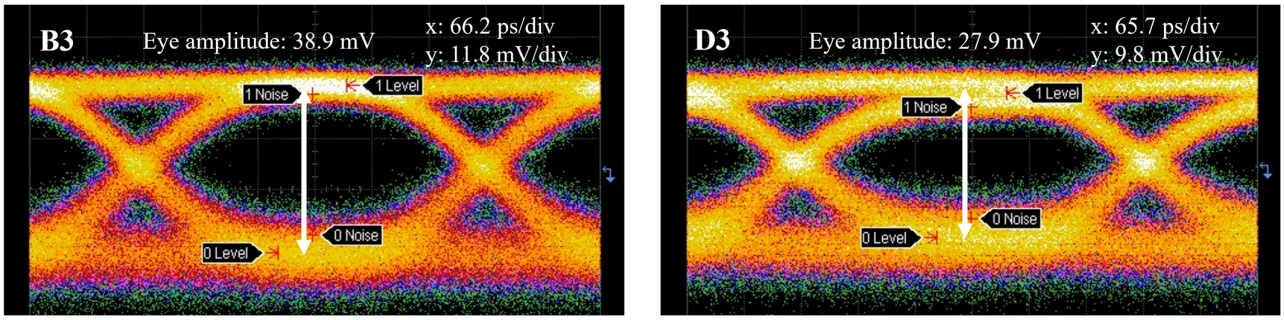

(**a**) (**b**)

Figure 9. 2.5 Gb/s eye-diagrams from receiver (**a**) B3 and (**b**) D3, measured without a limiting amplifier and at an optical power of −40 dBm.

4.4. Equivalent Space Mission

To assess the potential of using InGaAs/AlGaAsSb APD receivers in space applications, Displacement Damage Dose curves for InGaAs in LEO (800 km, 98° and 10 years), GEO (35,784 km and 15 years) and GPS (23,222 km, 56° and 12 years) were computed with the OMERE 5.9.3 [27]. Displacement damage dose versus aluminum shielding thickness is shown in Figure 10. At the proton energy of 62 MeV, the maximum displacement damage dose of 3.84×10^7 MeV/g (used in this work) covers typical LEO, GPS and GEO internal accommodations. Since P_{opt} of the receivers containing InGaAs/AlGaAsSb APDs did not show noticeable degradation, our results suggest they can be used in LEO, GPS, and GEO orbits.

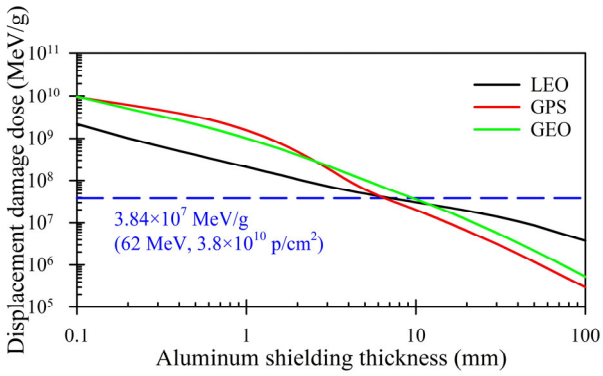

Figure 10. Displacement damage dose versus aluminum shielding thickness for InGaAs in LEO, GPS and GEO. The reference line (dashed line) indicates the condition used in this work (62 MeV proton at maximum fluence of 3.8×10^{10} p/cm^2).

Due to the safety measure, the post-rad characterizations were performed five weeks after the irradiation campaign. Therefore, possible room-temperature annealing of radiation-

induced defects may have occurred during this interval. As a result, our post-irradiation dark current, gain, and BER should be interpreted as values after five weeks of room-temperature storage rather than immediate post-irradiation characteristics.

We also note that the receivers were irradiated unbiased and at room temperature. When deployed in space applications, operation may involve different bias voltages, temperatures, and mission-dependent radiation conditions. Therefore, more extensive study would be beneficial.

5. Conclusions

Radiation hardness of 2.5 Gb/s optical receivers consisting of InGaAs/AlGaAsSb APDs integrated with TIAs was experimentally evaluated, through comparisons of the APDs' dark current, photocurrent, and avalanche gain as well as the receivers' BER data prior to and after proton irradiation. A total of 13 receivers were used, covering the control group and three proton fluences (3.8×10^9 to 3.8×10^{10} p/cm^2) representative of space environments.

After proton irradiation, despite increased dark current at reverse bias above 40 V, the APD's photocurrent and gain remain unchanged. Similarly, BER data showed no degradation, with the receiver's bandwidth exceeding 1.5 GHz required for 2.5 Gb/s operation. At 2.5 Gb/s data rate and 1550 nm wavelength, the irradiated receivers achieved a BER of 10^{-9} with an average input optical power of -38.2 ± 0.2 dBm, outperforming selected commercial receivers by 3.2–3.5 dB. Therefore, 62 MeV proton irradiation up to a fluence of 3.8×10^{10} p/cm^2 does not degrade the performance of optical receivers based on InGaAs/AlGaAsSb APDs. This suggests InGaAs/AlGaAsSb APDs have sufficient radiation hardness to be employed in 2.5 Gb/s optical communication links in LEO, GPS orbit, and GEO.

Author Contributions: Conceptualization, C.H.T. and J.S.N.; methodology, A.S., O.S.-P., C.H.T. and J.S.N.; software, D.C.; validation, D.C.; formal analysis, D.C., A.S. and O.S.-P.; investigation, D.C., J.V. and J.P.; resources, C.H.T. and J.S.N.; data curation, D.C. and J.V.; writing—original draft preparation, D.C. and C.H.T.; writing—review and editing, C.H.T., J.S.N. and J.P.; visualization, D.C., C.H.T. and J.S.N.; supervision, C.H.T.; project administration, C.H.T. and J.S.N.; funding acquisition, C.H.T. and J.S.N. All authors have read and agreed to the published version of the manuscript.

Funding: This work was supported by the European Space Agency under contract no. 4000143382/23/UK/AL (ARTES 4.0 Strategic Programme Line—Optical Communication Scylight).

Data Availability Statement: The original data presented in this study are openly available in the University of Sheffield ORDA database at https://doi.org/10.15131/shef.data.31972182.

Acknowledgments: Phlux Technology Ltd. (UK) is acknowledged for the supply of APD-TIA receivers.

Conflicts of Interest: Authors Anne Samaras and Oliver Saint-Pe were employed by the company Airbus Defence and Space. The remaining authors declare that the research was conducted in the absence of any commercial or financial relationships that could be construed as a potential conflict of interest.

Abbreviations

The following abbreviations are used in this manuscript:

AlGaAsSb	Aluminum Gallium Arsenide Antimonide
APD	Avalanche Photodiode
BER	Bit Error Rate
BERT	Bit Error Rate Tester
DDD	Displacement Damage Dose

EDRS	European Data Relay System
ESA	European Space Agency
FSOC	Free Space Optical Communication
GEO	Geostationary Orbit
GPS	Global Positioning System
InAlAs	Indium Aluminum Arsenide
InGaAs	Indium Gallium Arsenide
InP	Indium Phosphide
LC	Lucent Connector
LEO	Low Earth Orbit
NIEL	Non-Ionizing Energy Loss
PCB	Printed Circuit Board
RF	Radio Frequency
Si	Silicon
SMU	Source Measure Unit
SNR	Signal to Noise Ratio
TIA	Transimpedance Amplifier
VOA	Variable Optical Attenuator

References

1. Khalighi, M.-A.; Uysal, M. Survey on Free Space Optical Communication: A Communication Theory Perspective. *IEEE Commun. Surv. Tutor.* **2014**, *16*, 2231–2258. [CrossRef]
2. European Data Relay System (EDRS): Overview. Available online: https://www.esa.int/Applications/Connectivity_and_Secure_Communications/EDRS/Overview (accessed on 17 April 2026).
3. Free-Space Optical Backhaul for 5G Networks. Available online: https://connectivity.esa.int/archives/projects/free-space-optical-backhaul-5g-networks (accessed on 17 April 2026).
4. Richard, J.-C.; Poulenard, S.; Gnata, X.; Coret, L.; Anfray, T.; Crosnier, M.; Marduela, T.; Zurawski, L.; Montignaud, S.; Lacoste, F.; et al. In-orbit testing of GEO feeder links with TELEO. In Proceedings of the International Conference on Space Optics (ICSO 2024), Antibes Juan-les-Pins, France, 21–25 October 2024; pp. 58–78.
5. Védrenne, N.; Montmerle-Bonnefois, A.; Petit, C.; Chalali, E.; Lai-Tim, Y.; Krafft, L.; Henrion, J.; Houy, J.; Gustave, F.; Caillault, K.; et al. First results of ground to GEO optical links channel monitoring with FEELINGS. In Proceedings of the International Conference on Space Optics (ICSO 2024), Antibes Juan-les-Pins, France, 21–25 October 2024; pp. 282–292.
6. Propagation Data Required for the Design of Earth-Space Systems Operating Between 20 THz and 375 THz. Available online: https://www.itu.int/dms_pubrec/itu-r/rec/p/R-REC-P.1621-2-201507-I!!PDF-E.pdf (accessed on 17 April 2026).
7. Hamamatsu InGaAs APD G8931 Series. Available online: https://www.hamamatsu.com/content/dam/hamamatsu-photonics/sites/documents/99_SALES_LIBRARY/ssd/g8931_series_kapd1018e.pdf (accessed on 17 April 2026).
8. Goh, Y.L.; Marshall, A.R.J.; Massey, D.J.; Ng, J.S.; Tan, C.H.; Hopkinson, M.; David, J.P.R.; Jones, S.K.; Button, C.C.; Pinches, S.M. Excess Avalanche Noise in $In_{0.52}Al_{0.48}As$. *IEEE J. Quantum Electron.* **2007**, *43*, 503–507. [CrossRef]
9. Veitch, J.; Chen, D.; Petticrew, J.; Ng, J.S.; Tan, C.H. Sensitivity Improvement of 2.5 Gb/s Receivers Using AlGaAsSb Avalanche Photodiodes. *Appl. Sci.* **2025**, *15*, 12056. [CrossRef]
10. Taylor-Mew, J.D.; Petticrew, J.D.; Tan, C.H.; Ng, J.S. Simulation of $Al_{0.85}Ga_{0.15}As_{0.56}Sb_{0.44}$ avalanche photodiodes. *Opt. Express* **2022**, *30*, 17946. [CrossRef] [PubMed]
11. Sheridan, B.; Collins, X.; Taylor-Mew, J.; White, B.; Ng, J.S.; Tan, C.H. An extremely low noise-equivalent power photoreceiver using high-gain InGaAs/AlGaAsSb APDs. *J. Light. Technol.* **2025**, *43*, 741–746. [CrossRef]
12. Taylor-Mew, J.; Li, L.; Blain, T.; Tan, C.H.; Ng, J.S. Room Temperature InGaAs/AlGaAsSb Single Photon Avalanche Diode. *IEEE Photonics J.* **2025**, *17*, 1–6. [CrossRef]
13. ConeXpress Orbital Life Extension Vehicle: A Commercial Service for Telecommunications Satellites. Available online: https://www.esa.int/esapub/bulletin/bulletin127/bul127h_caswell.pdf (accessed on 17 April 2026).
14. Holmes-Siedle, A.; Adams, L. Radiation environments. In *Handbook of Radiation Effects*, 2nd ed.; Oxford University Press: Oxford, UK, 2002; pp. 18–19.
15. Stassinopoulos, E.G.; Raymond, J.P. The space radiation environment for electronics. *Proc. IEEE* **1988**, *76*, 1423–1442. [CrossRef]
16. Practices for Generating Space Environment Specifications with Modern Tools. Available online: https://aerospace.org/sites/default/files/2023-08/Best%20Practices%20for%20Generating%20Space%20Environment%20Specifications%20TOR-2022-00016.pdf (accessed on 17 April 2026).

17. Joshi, A.M.; Datta, S.; Miller, R.; Soni, N.; D'Angiolillo, M.; Mertz, J.; Sivertz, M.; Rusek, A.; Jardine, J. Proton and gamma radiation testing of 10 GHz bandwidth, uncooled, linear InGaAs optical receivers. In Proceedings of the Sensors and Systems for Space Applications XII, Baltimore, MD, USA, 14–18 April 2019; pp. 117–128.
18. Olantera, L.; Bottom, F.; Kraxner, A.; Detraz, S.; Menouni, M.; Moreira, P.; Scarcella, C.; Sigaud, C.; Soos, C.; Troska, J.; et al. Radiation Effects on High-Speed InGaAs Photodiodes. *IEEE Trans. Nucl. Sci.* **2019**, *66*, 1663–1670. [CrossRef]
19. Becker, H.N.; Johnston, A.H. Dark current degradation of near infrared avalanche photodiodes from proton irradiation. *IEEE Trans. Nucl. Sci.* **2004**, *51*, 3572–3578. [CrossRef]
20. Collins, X.; Sheridan, B.; Price, D.; Cao, Y.; Blain, T.; Ng, J.S.; Tan, C.H.; White, B. Low-noise AlGaAsSb avalanche photodiodes for 1550 nm light detection. In Proceedings of the Optical Components and Materials XX, San Francisco, CA, USA, 14 March 2023.
21. Product Datasheet CGY2102UH/C2 2.5 Gb/s Transimpedance Amplifier. Available online: https://fregat.ru/upload/iblock/675/x59np4x81gnfa8d1csrix3sqcuvzjxpd.pdf (accessed on 17 April 2026).
22. ESA European Preferred Parts List (Issue 51). Available online: https://escies.org/webdocument/showArticle?id=166&groupid=6 (accessed on 17 April 2026).
23. Yan, G.; Bi, J.; Xu, G.; Xi, K.; Li, B.; Fan, L.; Yin, H. Simulation of total ionizing dose (TID) effects mitigation technique for 22 nm fully-depleted silicon-on-insulator (FDSOI) transistor. *IEEE Access* **2020**, *8*, 154898–154905. [CrossRef]
24. Inguimbert, C.; Gigante, R. NEMO: A code to compute NIEL of protons, neutrons, electrons and heavy ions. In Proceedings of the 8th European Conference on Radiation and Its Effects on Components and Systems (RADECS 2005), Cap d'Agde, France, 19–23 September 2005; pp. PG2-1–PG2-8.
25. GoFoton InGaAs Avalanche Photodiode (APD) 2.5 Gbps APD with TIA. Available online: http://gofoton.cn/products/optics/materials/apd_tia.html (accessed on 17 April 2026).
26. Dexerials InGaAs APD-TIA Receivers KPDXA2GK-H33. Available online: https://www.dexerials.jp/asset/optical_semiconductor/products/kpdxa2gk-h33/kpdxa2gk-h33_en.pdf (accessed on 17 April 2026).
27. Peyrard, P.F.; Beutier, T.; Serres, O.; Chatry, C.; Ecoffet, R.; Rolland, G.; Boscher, D.; Bourdarie, S.; Inguimbert, C.; Calvel, P.; et al. OMERE 2.0: A toolkit for space environment. In Proceedings of the Radiation and Its Effects on Components and Systems (RADECS 2003), Noordwijk, The Netherlands, 15–19 September 2003; pp. 639–641.

Disclaimer/Publisher's Note: The statements, opinions and data contained in all publications are solely those of the individual author(s) and contributor(s) and not of MDPI and/or the editor(s). MDPI and/or the editor(s) disclaim responsibility for any injury to people or property resulting from any ideas, methods, instructions or products referred to in the content.